Published in final edited form as:
J Neural Eng. 2009 October ; 6(5): 055007. doi:10.1088/1741-2560/6/5/055007.

Integrated device for optical stimulation and spatiotemporal electrical recording of neural activity in light-sensitized brain tissue

Jiayi Zhang[1], **Farah Laiwalla**[2], **Jennifer A Kim**[3], **Hayato Urabe**[2], **Rick Van Wagenen**[4], **Yoon-Kyu Song**[2], **Barry W Connors**[3], **Feng Zhang**[5], **Karl Deisseroth**[5], and **Arto V Nurmikko**[1,2]

Jiayi Zhang: zhangf@stanford.edu; Karl Deisseroth: dessero@stanford.edu; Arto V Nurmikko: Arto_Nurmikko@brown.edu

[1]Department of Physics, Brown University, Providence, RI 02912, USA

[2]Division of Engineering, Brown University, Providence, RI 02912, USA

[3]Department of Neuroscience, Brown University, Providence, RI 02912, USA

[4]Blackrock Microsystems, 391 Chipeta Way, Salt Lake City, UT, USA

[5]Department of Bioengineering and Psychiatry, Stanford University, CA, USA

Abstract

Neural stimulation with high spatial and temporal precision is desirable both for studying the real-time dynamics of neural networks and for prospective clinical treatment of neurological diseases. Optical stimulation of genetically targeted neurons expressing the light sensitive channel protein *Channelrhodopsin* (ChR2) has recently been reported as a means for millisecond temporal control of neuronal spiking activities with cell-type selectivity. This offers the prospect of enabling local delivery of optical stimulation and the simultaneous monitoring of the neural activity by electrophysiological means, both in the vicinity of and distant to the stimulation site. We report here a novel dual-modality hybrid device, which consists of a tapered coaxial optical waveguide (‘optrode’) integrated into a 100 element intra-cortical multi-electrode recording array. We first demonstrate the dual optical delivery and electrical recording capability of the single optrode in *in vitro* preparations of mouse retina, photo-stimulating the native retinal photoreceptors while recording light-responsive activities from ganglion cells. The dual-modality array device was then used in ChR2 transfected mouse brain slices. Specifically, epileptiform events were reliably optically triggered by the optrode and their spatiotemporal patterns were simultaneously recorded by the multi-electrode array.

1. Introduction

How does spatially focused neural stimulation affect the activity of local and distant neurons, possibly leading to alterations in behavior and changes in disease states? This question not only encompasses a fundamental concern in the field of neural circuit dynamics, but is also central to the quest for innovative treatments of neurological disease, rooted in better scientific understanding of the mechanisms of neural function and dysfunction. The ability to answer this and other related questions requires tools enabling selective neural stimulation coupled with simultaneous high-resolution spatiotemporal recording.

Neural stimulation by means of injecting electrical current through brain tissue has been a powerful tool in electrophysiology [17] and clinical neuroscience [33,38], in spite of the uncertainties associated with complex current paths, non-selective depolarization of axons, dendrites and neuronal cell bodies by the complex current pathways [10,26]. Direct optical stimulation of neural cells in brain tissue genetically modified by expressing channelrhodopsin-2 (ChR2) has recently been achieved [11,35,56] and applied in both *in vitro* and *in vivo* studies [2,29,39,57]. This new kind of 'optogenetic' stimulation technique can genetically be customized to target specific types of neurons with sub-millisecond temporal precision [2]. Various light delivery schemes have been reported, to match the excitation spectrum of ChR2 in the blue, including band-filtered white light [11,56], light emitting diodes (LED) [12] or laser-coupled optics [39] for *in vitro* applications, as well as direct epicranial LED implantation [29] for *in vivo* applications. In broader terms of tools that have been applied by using optical fiber based endoscopic technologies in neuroscience, these have been so far mostly employed for structural imaging such as light delivery for fluorescence or 2-photon imaging [20,21,41] and functional imaging such as optical coupling between light sources and photo-detectors in functional optical coherence tomography (fOCT) [31]. The recent development of optogenetics methodology has opened avenues for optical fiber based neuronal stimulation including *in vivo* applications [2,4]. So far, the spatial distribution of the stimulating light using these delivery schemes at the target brain tissue has been limited by the divergence of the light source itself or the numerical apertures of the optical instruments, further 'blurred' by scattering intrinsic to the tissue. Moreover, recording of the evoked neural activity has been limited to single patch or EEG/EMG [2] recordings. A mechanically simple construct of an optical fiber glued to an extracellular electrode has recently been reported [23] to monitor neuronal activity evoked by optical stimulation in ChR2 transfected mice. Elsewhere, a variety of techniques has been developed to record from a large population of neurons with high spatiotemporal resolution, ranging from multi-electrode arrays [25,51] to optical imaging methods [24]. The multi-electrode arrays do not easily allow for specific stimulation of neural electrical activity due to the presence of electrical artifacts etc. Meanwhile, the optical imaging methods such as intrinsic optical signal detection are technically challenging for detailed tracking of spiking activity in local intra-cortical microcircuits.

A paradigm case of extended neural circuit phenomena where space- and time-dependent excitation/recording is important is epileptic activity. Epileptiform activity in disinhibited brain tissue is characterized by synchronized population firing, and occurs predominantly in parts of the brain with high degrees of recurrent excitatory circuitry, such as the neocortex and hippocampus [52]. The initiation and propagation of such activity is fairly well understood with a simple neuronal network model, utilizing the pattern of connectivity among these neural populations [49,50]. One-dimensional recordings of the epileptiform wave in neocortical slices have been demonstrated previously by linear microwire arrays [14–16,40], revealing the patterns of wave initiation and propagation across the columnar and laminar architectures in neocortex. It is thus interesting to study the two-dimensional or even three-dimensional spatiotemporal propagation patterns, including those under pharmacologically induced seizure conditions. Calcium imaging has been used to record single neuron activities but with a limited neural circuit recording area [5]. In this paper we use the two-dimensional spatiotemporal propagation of epileptiform activity as an example of the application of a newly developed set of tools.

Below we describe a tapered coaxial optical waveguide construct, dubbed as the 'optrode', which, after a range of testing and characterization, is embedded within a 100-element 'Utah' intra-cortical multi-electrode recording array (MEA) [13,30]. This dual-modality, hybrid, optrode–MEA device is capable of locally delivering light stimuli to neural tissue while simultaneously multisite recording extracellular activities from an area of

approximately 4.0 mm × 4.0 mm around the stimulation focus (these are present dimensions —with extended MEA and optrode fabrication techniques any combinations and many geometries are possible). The optrode itself is a dual-device element providing simultaneous light delivery and electrical recording capabilities. As described below, we first tested the single optrode as a stand-alone unit in the intrinsically photosensitive mouse retina. Green laser light was delivered through the optrode to trigger retinal photoreceptors, and the light-induced change of spike activity was recorded from retinal ganglion cells via the integrated electrical pathway of the optrode. In a different validation and evaluation step, mouse brain slices with cortical neurons rendered light sensitive by viral transfection via ChR2 also showed direct blue light-triggered action potentials upon being stimulated by the stand-alone optrode. Next, and most important to this paper, the optrode–MEA dual function array device was used to study the 2D spatiotemporal propagation of optically induced epileptic waves in disinhibited ChR2 mouse cortical slices. Epileptic waves with robust propagation patterns were demonstrated.

2. Single optrode fabrication and its optical characteristics

2.1. Fabrication procedure of single optrode and methods

The single optrode is a tapered glass optical fiber with a sub-micron-sized aperture at its tip formed by gold metallization cladding (schematic in figure 1(a)). It was fabricated from a multimode optical fiber (Fiber Instrument Sales Inc., 62.5 μm core, 125 μm cladding), whose bare end was cleaved and cleaned with isopropanol before further processing, to remove organic substances on the optical fiber after stripping the outer polymer jacket. The tapered end of the fiber was created by wet etching in aqueous hydrofluoric acid (HF, 49%) at room temperature (22–24 °C). The fiber was immersed into the etching solution perpendicular to the surface of the solution and pulled out at a speed of 20 μm min^{-1} until a sharp taper was formed. Different tip angles can be formed by controlling the rate at which the fiber is withdrawn from the etching solution. (Alternatively, organic solvents can be used to serve as an immiscible protection layer to the aqueous HF for static etching, where the tip angle is created at the HF/organic solvent interface [28]). The etched optical fiber was then rinsed in de-ionized water and a 500 nm thick gold film was deposited on the tapered surface using a high vacuum thermal evaporator (Angstrom Engineering). The chosen deposition angle was 27° while the optrode was rotated at a speed of 12π rad min^{-1}. A magnet wire (Alpha Wire Company) was attached to the metalized part of the optrode by means of silver epoxy (H20E; Epoxy Technology) and served as the electrical conduit to external recording electronics. With the exception of the final 50 μm of the tapered tip, the metalized part of the fiber was insulated using a UV-curable epoxy (Norland Optical Adhesive 74). Figure 1(b) shows scanning electron microscope (SEM) images of an optrode tip. The exposed metallic part of the optrode has micron-size facets, which were created during chemical etching. The lower image in figure 1(b) shows the geometry and character of the optical aperture and the adjacent thermally evaporated grains of the gold metal. The integrity of the insulation layer was validated by measuring the electrical impedance of the optrode (see details in section 3.3 below) at different submersion depths in phosphate buffer solution (PBS). We have demonstrated (data not shown) that the electrical impedance of the optrode remains the same when the tip and the insulated part of the optrode is gradually lowered into the PBS.

The fluorescence and bright field images of the optrode were obtained using a CCD camera (Dage-MTI) and captured using Videum Capture (Winnov). Image J (Image Processing and Analysis in Java, NIH) was used for obtaining gray scale distributions from images and converting them to light intensity profiles. The Gaussian fits for the curves were done in Origin (OriginLab).

In the following, all data in the text are presented as mean ± standard deviation. Error bars in the figures are standard deviations.

2.2. Optical characteristics of a single optrode

The optrode construct demonstrated in this paper is essentially an optical waveguide structure terminating in a sub-micron-sized aperture, not unlike those which are employed as sub-wavelength light sources or fluorescence probes in near field optical microscopes (NSOM) [32,42]. In NSOM applications, which are not the subject here, it can be possible to reach nanometer scale lateral spatial resolution [8]. Then, since the apertures of these probes are required to be as small as 50 nm, their optical throughput is quite small, on the order of 10^{-5}. Here, in order to maximize the amount of light delivered to the brain tissue while maintaining a 'point source' and control the light delivery scheme, the optical aperture of the optrode was designed to be larger (in the 1 μm range). Starting from the core diameter of the initial silica optical fiber of 62.5 μm, we nonetheless have to completely remove the cladding in preparing the tapered end of the optrode. A sizable fraction of the light originally confined in the core was then lost through the sidewalls of the optrode tip, yet limited by the presence of the conductive coating at the end of the taper. The known and measured (by us) absorption of 100 nm Au thin films for 1.5 mW incident light at 404 nm is 0.812.

The optical output from the optrode can be analyzed with a model similar to that for an NSOM probe. Bethe addressed this problem by solving Maxwell's equations for the diffraction of electromagnetic radiation by a circular hole in an infinitely thin and perfectly conducting screen [7], where the size of the circular hole is smaller than the wavelength of light (i.e., $ka \ll 1$, $k = 2\pi/\lambda$, a is the diameter of the aperture). The far field radiation of the aperture can be treated as a combination of two radiating dipoles located at the center of the aperture. The size of the optrode aperture is comparable to the wavelength ($ka \sim 1$); the far field radiation can thus be calculated similarly and shows Gaussian distribution according to recent computational analysis [3,18,37]. To quantify the optical throughput of the optrode in a non-scattering medium, the optrode was placed in Rhodamine-6G (R6G, Sigma Aldrich) solution, while light from a green laser (532 nm; World Star Tech) was coupled into the far end of the fiber for fluorescence excitation. Figure 2(a) is a fluorescence image of the optrode output in the Rhodamine-6G solution, where the intensity profiles were taken at two planes perpendicular (short axis) and along (long axis) the optrode. The intensity profiles along the two axes and the Gaussian fit curves are shown in figure 2(b). The variances for the Gaussian fits are 18 μm for long axis ($d_{\text{longaxis-R6G}}$) and 13 μm ($d_{\text{shortaxis-R6G}}$) for short axis. While distribution along the short axis is due to the angular dependence of transmitted light from the aperture [37], the long axis optical output is determined by both the throughput from the aperture (forward direction) and the transmitted light from the Au thin film at the optrode tip (backward direction). The estimated throughput from the aperture is the same as the transmitted throughput from a planar Au thin film of the same thickness (data not shown). The overall optical output can be approximated as a prolate spheroid, whose eccentricity is 0.692.

The light scattering properties of the brain tissue can vary vastly depending on species [4,55], incident wavelengths [55], physiological status of the tissue [9,55] and even the age of the subject. To quantify the optical output in the light scattering brain tissue, the optrode was placed in brain tissue in P28 mouse brain slices (for consistency with the brain slice experiments as described below) and a blue laser diode (440 nm; Nichia Corp., within a homemade package) was coupled to the fiber end of the optrode. Figure 2(c) shows a DIC image of the scattered light from the optrode in such tissue. The optrode was placed at a penetration depth of around 50 μm from the surface of the slice. Only the intensity distribution along the short axis is shown, because the 'shadow' of the optrode impeded optical access to the long axis. The 'noise' in the light intensity profile in figure 2(d) is

larger than that in figure 2(b), thereby highlighting the effects due to scattering in the brain tissue. The variance for the Gaussian fit ($d_{\text{shortaxis-tissue}}$) is 18 μm, larger than that of the corresponding solution case ($d_{\text{shortaxis-R6G}} \sim 13$ μm in the Rhodamine-6G fluorescence image). The variance for the long axis $d_{\text{longaxis-tissue}}$ can be calculated from the eccentricity of the prolate spheroid obtained previously. Assuming that the excitation light intensity at the full width half maximum (FWHM) is adjusted for the threshold of inducing ChR2 spikes, the total volume for the prolate spheroid is

$$V_{\text{spheroid}} = \frac{4}{3}\pi\, d_{\text{longaxis-tissue}} d^2_{\text{shortaxis-tissue}}, \quad (1)$$

which defines the initial excitation volume as 3.4×10^4 μm^3.

3. Single optrode performance testing: experiments in mouse retina

3.1. Mouse retina preparation and electrophysiology

All procedures were in accordance with National Institutes of Health guidelines and approved by the Institutional Animal Care and Use Committee (IACUC) at Brown University. Adult wild-type C57Bl6 mice were euthanized by over exposure to carbon dioxide and enucleated bilaterally. The retinae were dissected out in Ames' medium (A1420, Sigma Aldrich, with 21 mM $NaHCO_3$ and 10 mM glucose) equilibrated with 95% O_2, 5% CO_2. Dark adaptation of the retinae was conducted for 60 min before they were mounted on nitrocellulose filter paper (0.47 μm pore, Millipore Corp.) and placed in a liquid–gas interface recording chamber system with the ganglion cells facing up. Figure 3(a) shows the experimental setup for the retina stimulation/recordings. Both a halogen lamp and a 532 nm green laser were used to stimulate the retina. Incident light power levels between 500 μW and 5 mW (measured by calibrated power meter) were used without bleaching the retinal photoreceptors. The halogen white light source was coupled to a fiber guide and placed right below the recording chamber. An optrode, mounted on a 3D micromanipulator, was inserted into the retina until spikes were detected. The extracellular potential from the optrode (i.e., recorded by its conductive cladding), with reference to a Ag/AgCl wire in the bath, was preamplified (1000 gain, 1–10 kHz bandpass; Low Noise Preamplifer Iso-DAM8, World Precision Instruments). Raw data (10 kHz sampling rate) were then acquired using Labview (National Instruments™). All the spikes were thresholded at −300 μV (250 Hz–4.8 kHz) and overlaid in a 2 ms window using Matlab. The spike rasters were obtained using a Matlab program as well.

The electrical impedance spectrum of the optrode was measured using a setup consisting of a digital function generator and an oscilloscope. The evoked spike waveforms of the ganglion cells were analyzed with custom programs written in Matlab (The Mathworks, Inc™) in the retina experiments.

3.2. Dual optical stimulation and electrical recording by the optrode in mouse retina

The stand-alone single optrode's capability for optical stimulation and electrical recording was demonstrated in intrinsically light sensitive tissue—i.e., the mouse retina. Since the ganglion cells are formed as a single-cell layer, most retinal recordings are conducted using planar multielectrode arrays [19,48]. However the electrical contact between the ganglion cell and the planar electrode is difficult to control. Using our optrode with its tapered structure, spiking activities from multiple ganglion cells could readily be recorded. Both halogen white light and green (532 nm) laser light could transit through the whole retinal tissue preparation. In the first set of control experiments, the wide area white light illumination (not through the optical fiber) was used to stimulate the retinal tissue for the

duration of ~2.5 s and ganglion cell responses were recorded using the single optrode as shown in the raster plots of figure 3(b). Robust spiking activity was triggered for 2–3 s after the light was turned off; this is the characteristic of an OFF-transient ganglion cell (In one of the traces, turning the light on triggered several spikes as well). In the second set of experiments, the green laser was coupled into the optrode via its fiber end to stimulate the retinal tissue for ~2 s. In this case the optrode was used to simultaneously record the ganglion cell responses (raster plots of figure 3(c)). Spiking activity was triggered by turning the laser light both on and off.

3.3. Electrical recording characteristics of optrodes in mouse retina

As noted, the design of the single optrode element had two objectives: the local delivery of light stimulation and the simultaneous electrical recording of proximal, associated neuronal activity suitable for both *in vitro* and *in vivo* applications. The electrical impedance of the optrode determines the bandwidth and the root-mean-square noise, thus its capability for extracellular electrophysiological recordings of neural activities. Figure 4(a) shows the average impedance spectrum of eight separately fabricated optrodes. The plot here refers to the absolute value of the impedance (a Bode plot). A simple quantitative model of the electrode has been analyzed by Robinson [43], where the equivalent circuit of a metal microelectrode has the following impedance

$$Z_{\text{electrode}} = R_s + R_m + \frac{1}{j\omega C_s} + \frac{R_e}{1 + j\omega R_e C_e}, \tag{2}$$

where R_s is the resistance of the (saline) bath between the metallic interface and infinity, R_m is the resistance of the metallic portion of the electrode, C_s is the shunt capacitance from the tip to the amplifier input, ω is the frequency of the electric field, R_e is the leakage resistance in the electric double layer, C_e is the capacitance of the electric double layer, and j is the complex constant. There are two major contributions to time constants in the impedance spectrum, one from the double layer and the other between the electrode and the amplifier (shunt capacitance). By plotting equation (2) using Mathematica (Wolfram Research), one can find that the shunt capacitance dominates the time constant of the optrode. The double exponential decay fit of the impedance spectrum in figure 4(a) gives two decay constants: 2628 and 87.6 s^{-1}, which is consistent with Robinson's model. The electrical impedance is relatively invariant in the frequency range relevant for electrophysiological neural recordings respectively, enabling access to both high frequency 'spikes' and lower frequency local field potentials with high fidelity.

Figure 4(b) shows 24 spontaneous spike waveforms recorded by the optrode from mouse retinae, overlaid in a 2 ms window. The consistency of both the shapes and the amplitudes of the waveforms indicate that these are single-unit spiking activity from one ganglion cell. The peak-to-peak amplitudes of the spikes V_{pp} are between 100 and 500 μV. A raw data trace of the retina recordings is shown in figure 4(c). The V_{rms} for the noise is 14.3 μV, while the standard deviation V_{std} is 44.6 μV. The signal-to-noise ratio (SNR) of an electrode is calculated as [36]

$$\text{SNR} = V_{\text{pp}}/2 \cdot V_{\text{std}}. \tag{3}$$

Thus, the SNR for the optrode-recorded spikes lies between the values of 1.12 and 5.60 for the present structures (which are not yet fully optimized).

4. Single optrode stimulation of ChR2-expressing neurons in cortical slice (with patch clamp recording)

4.1. Lentivirus production, transduction and stereotactic viral delivery for optogenetic transfection

pLenti-Synapsin-hChR2(H134R)-EYFP-WPRE DNA was amplified in our laboratories using standard molecular biology techniques. The plasmid housed both the ChR2 and yellow fluorescent protein (EYFP) for purposes of imaging the transfected brain tissue.

Postnatal day14 mice (CD-1 Charles River) were anesthetized by intraperitoneal injections of ketamine (70 mg/kg) and Dormitor (0.5 mg/kg) cocktail. The head of the animal was placed in a stereotactic apparatus (David Kopf Instruments) and a craniotomy was drilled (anteroposterior, 0 mm from bregma; lateral, 3 mm; ventral, 0.85 mm). Concentrated lentivirus solution (0.5 μL) was injected at the desired stereotactic locus at a speed of 0.05 μL min^{-1} using a programmable pump (PHD2000, Harvard Apparatus). The skin on the skull was sutured up and Antisedan (0.5 mg/kg) was given to the animal at the conclusion of the surgery.

4.2. Mouse brain slice electrophysiology and photostimulation

Two weeks after the lentiviral injection, the animals were sacrificed and 350 μm thick coronal cortical slices were prepared using a vibratome (VT 1000; Leica) in ice cold artificial cerebrospinal fluid (ACSF, containing 126 mM NaCl, 3 mM KCl, 1.25 mM NaH_2PO_4, 2 mM $MgSO_4$–$7H_2O$, 26 mM $NaHCO_3$, 10 mM dextrose and 2 mM $CaCl_2$ equilibrated with 95% O_2 and 5% CO_2). A fluorescence stereomicroscope (GFP filter set, 0.75–11.25X, Nikon Instrument) with a plan apochromat objective (1×, 0.04 NA, Nikon Instrument) was used for low-magnification fluorescence images of the whole slice. The exposure time to the fluorescent excitation light was kept below 5 s to minimize the unnecessary excitation of ChR2-expressing neurons. Patch recordings were performed in a whole-cell current clamp configuration using Axoclamp 2B (Axon Instrument) at room temperature (22–24 °C). The cells were visualized in a fixed-stage infrared differential interference contrast (DIC) microscope. ChR2 expressing neurons were identified through the EYFP fluorescence embedded in the initial DNA plasmid (excitation wavelength range 489–505 nm, emission range 524–546 nm, Semrock filters) and patched with a borosilicate micropipette (4–8 MΩ resistance). The intracellular solution contained 130 mM potassium gluconate, 10 mM HEPES, 4 mM KCl, 2 mM NaCl, 0.2 mM EGTA, 4 mM magnesium ATP, 0.3 mM tris-GTP and 14 mM tris-phospocreatine (pH 7.25; 291 mOsm). The fiber far end of the optrode was directly coupled to the 440 nm blue laser diode, with pulse widths of up to 100 ms in duration and delivering approximately 0.85 mW throughput power. The electrophysiological spiking data were processed using ClampFit (Axon Instrument).

4.3. Single optrode stimulation of ChR2-expressing neurons

The excitability of ChR2 expressing pyramidal neurons by the single stand-alone optrode was characterized in a mouse cortical slice, where neural response was recorded of a single cell by patch-clamp methods. In the coronal cortical slice preparation, a uniform fluorescent region of about 300 μm width was identified in layer V/VI of the somatosensory cortex (figure 5(a)). No single fluorescent neurons were unambiguously observed due to the brightness of the background fluorescence. Most of the patched cells in the bright fluorescent region had light-triggered spiking responses when light was delivered through the water-immersion objective (control experiment data not shown). In the optrode experiment, a healthy neuron at the depth of about 50 μm in the fluorescent region was patched with a glass micropipette (figure 5(b)). The optrode was then moved to the surface

of the slice and lowered by a few micrometers such that the tip of the optrode was imbedded slightly inside the slice. We found typically that a 10 ms laser pulse of 3.3 mW peak power emanating from the optrode elicited spikes with firing probability of $P = 0.2$. One of such light-triggered spikes is shown in figure 5(c). The spike latency to the onset of the light stimulus was 9.7 ± 1.4 ms (figure 5(d)). Such evidence indicates that the 3.3 mW output power from the optrode is close to the threshold for eliciting spikes, given the reported steep relationship between spiking probability and laser power [39]. Since the optrode was about 50 μm from the recorded neuron, we can use equation (1) to estimate that the photoactivation volume created by the optrode is about 7.57×10^5 μm^3. By increasing both the power to 6.6 mW and the duration of the laser pulses to 100 ms, the optrode was able to reliably elicit multiple spikes from the same neuron (figure 5(e)).

5. Dual-modality-integrated optrode–MEA device: experiments in ChR2-expressing mouse cortical slices

5.1. Dual-modality optrode–MEA device fabrication and experiment arrangement for cortical slices

Figure 6(a) shows a schematic of the fully integrated optrode–MEA device. The starting 100-element MEA was fabricated by Blackrock Microsystems, based on the Utah array [13]. This multi-electrode array is a three-dimensional silicon-based structure made of a 10 × 10 grid of 1 mm long tapered microelectrodes based on a 4.2 mm × 4.2 mm × 0.2 mm thick substrate. The inter-electrode distance was 400 μm [36]. The array was then further processed as follows. Ablative laser machining and drilling were applied on the MEAs to remove one silicon electrode shank and to create a hole with a diameter of approximately 203 μm (Gateway Laser Services). The fiber optic optrode element was mechanically fixed through the hole with UV curable epoxy (Norland Optical Adhesive 74) so that its tip was precisely aligned in the plane of the tips of the Pt-coated silicon microelectrodes, and attached with thermally conductive epoxy (H70-E; Epoxy Technology) onto an aluminum rod. The electrical contact wires of the array are extended as a bundle from the side of the array (figure 6(b)). Figure 6(c) shows a close up view of the tips of the device. The shape and dimension of the optrode are seen to be similar to those of the other electrodes.

As an application of the new device construct, seizure wave propagation experiments were conducted in a liquid–gas interface recording chamber system in the presence of the $GABA_A$ receptor antagonist picrotoxin (PTX, 10 μM; Sigma Aldrich) at 32 °C. The PTX container was covered with dark foil to avoid decomposition due to the exposure of the photosensitive PTX to ambient light. The bath flow rate was 4 mL min^{-1}. Transfected slices were set on the black filter paper (HABP04700 Millipore) to avoid unwanted light scattering from the bottom of the chamber. The transfected ChR2 expression region was identified under the fluorescence stereomicroscope (figure 7). The optrode within the optrode–MEA device was first visually targeted to and then micro-positioned at the center of the transfected region. The plane of the microelectrode tips was aligned to be parallel to the surface of the brain slice, and the entire device array was inserted with a 50–100 μm penetration depth into the slice with the aid of a 3D micromanipulator. Epileptiform activity was evoked through the optrode using 500 μs duration laser (440 nm) pulses for excitation of the ChR2. We limited the typical inter-stimulus interval to about 1 min. A dedicated data acquisition system (Cerebus; Blackrock Microsystems) was used to capture the multichannel electrophysiological data at 10 kHz per channel. Variations in the amplitudes of seizure waves measured at different sites were partly due to impedance differences between electrodes. The onset time of the waves was determined by measuring the delay between stimulus and a triggered-wave voltage amplitude value of 150 μV [6]. Since the onset of the epileptiform activity was quite sharp, the threshold was a relatively accurate value for

different channels. Data plots and analysis were conducted using Matlab programs. Electrode placement was determined post-experimentally by Nissl staining of whole mount slices.

5.2. Spatiotemporal mapping of light-induced seizure wave by integrated optrode-MEA device in mouse brain slices

The functioning of the hybrid optrode–MEA device was verified in a disinhibited mouse cortical slice. The advantage of using this type of device for studying epileptiform wave propagation is that the activity from a large area of the neocortex and even other parts of the slice can in principle be simultaneously recorded. We note that for the specific MEA used here, with its 400 μm inter-electrode separation, the spatial resolution of the current device is poorer than e.g. in manually assembled 1D electrode arrays [15,16,40]. Since epileptiform waves are population bursts which require a majority of neurons to fire synchronously, it is necessary to 'externally bias' the intrinsic neuronal network. Different pharmacological methods can be used to block $GABA_A$ inhibitory synaptic transmission, including penicillin [45], bicuculline [52] and picrotoxin (PTX) [34]. We employed PTX in our cortical demonstration experiments because of its potency and stability. According to a previous study [14], increasing the concentration of PTX does not significantly change the wave velocity or amplitude once the wave has been initiated. A PTX concentration of 10 μM is near optimal for initiating single, robust epileptiform events. In our experiments, higher PTX concentrations tended to cause higher frequency of spontaneous events.

It has been shown that synaptic interactions are critical for synchronization of neuronal bursting activity [34,52]. In a neuronal network where the inhibitory synapses are blocked, the activation of a localized neural population can thus lead to bursting events propagating throughout the entire network. Electrical stimulation has been used to evoke epileptiform activity by passing a bipolar square current pulse (typically hundreds of μs long and ~10–100 μA in amplitude) through the disinhibited tissue. We hypothesized that direct optical stimulation of a small population of light-sensitive neurons should be able to evoke epileptiform waves as well. This assumption was tested in ChR2 transfected cortical slices, where the optrode–MEA device was used to study the 2D spatiotemporal propagation of optically induced epileptiform waves. Figure 7(a) shows the geographic location of each electrode in the fixed slice, which is identified from the 'markers'—mechanical holes created by the insertion of the electrodes into the tissue after the MEA removal. We chose to have the optrode deliver optical stimulation to layer II/III of the neocortex, whence approximately three rows of electrodes were able to record the activity in the cortical area in the left panel of figure 7(a). An enlarged view of the 'markers' in the right panel of figure 7(a) shows that the cells surrounding the electrodes were not adversely affected by the insertion of the electrodes. A fluorescent region of about 300 μm width was identified as the excitation target in the somatosensory cortex (figure 7(b), left panel). As shown in figure 7(b) right panel, the electrodes at the four corners of the array served as micro-positioning and electrical references; four of them immediately adjacent to the hole in one direction along the plane of the array were left unwired due to geometrical wiring constraints. This left approximately 92 microelectrodes in the array as being usable through a bundle of 25 μm diameter gold wires. The overlay of the spatial placement of the electrodes onto the fluorescent image shows that the optrode and four other electrodes were located in the fluorescent region. Each electrode is labeled by its row and column number. (We verified that electrodes in row 5 lay between layers I and IV, while those in row 6 lay mostly in the white band of layer V and those in row 7 are in the wide band of layer VI).

Optical stimulation pulses of 15 mW peak power into the fiber at 440 nm with duration of 500 μs were delivered to the center of the fluorescent region. Inter-stimulus intervals were about 60 s. Light-induced epileptiform events were not observed until at least 30 min after

the commencement of PTX flow. The spatiotemporal propagation of the epileptic waves was recorded by the multi-electrode array. For the hybrid unit used, the electrical impedances of the electrodes at 1 kHz across the array were on average 301 kΩ with a standard deviation of 369 kΩ. Figure 8(a) summarizes epileptic waves recorded by the electrodes in row 6 of the array (highlighted with red rectangle in figure 7(b), right panel). Photoelectric artifacts of the light stimulus (i.e., a microelectrode acting as a junction photodiode of sorts) could also be seen in different electrodes with different amplitudes. The electrode labeled by '0' in figure 8(a) lies right below the optrode, recording field potential events < 3 ms after the light was turned on, suggesting direct optical initiation of epileptic activity. The experimentally extracted velocity of the wave propagation from column 5 to column 1 was 3.3 ± 0.3 cm s^{-1} while that from column 5 to column 10 was 4.6 ± 0.1 cm s^{-1}. These values are comparable to those (7.4 ± 0.6 cm s^{-1}) in the literature [40]. Figure 8(b) shows two sample waveforms of the light-evoked seizure waves and that of a spontaneous wave. While the shapes of the waveforms were identical, the propagation patterns acquired by the 2D array are completely different. In particular, the light-evoked epileptic waves have similar spatiotemporal propagation in different runs (details in figure 9), while the spontaneous waves propagate in an unpredictable way (data not shown). The details of the 2D spatiotemporal propagation of the light-evoked epileptiform activity are shown in figure 8(c), aimed at demonstrating the utility of our hybrid optrode–MEA device. The $T = 78.45$ s frame shows the activity of the slice before the light stimulus was turned on. A negative deflection of 300 μV was detected at 400 μm below the optrode (row 6 column 5) at $T = 78.46$ s, 5ms after the onset of the stimulus. Such a delay indicates that the recorded event is a propagating epileptic wave instead of direct depolarization due to the stimulation light pulse. Thus, the data suggest that the optical stimulation was localized in the vicinity of the optrode without directly affecting neighboring electrodes. Large epileptic waves of >400 μV were observed to be propagating rightward from the optrode along rows 5 and 6 between $T = 78.46$ s and $T = 78.51$ s. There was persistent activity in columns 6 and 7 at $T = 78.52$ s and $T = 78.53$ s. On the other hand, the waves propagating leftward from the optrode had much smaller amplitudes. This is consistent with previous observations that the propagation of cortical epileptic waves is direction sensitive [15]. In addition, the amplitudes of the waves propagating in layer VI (recorded by row 7) were much smaller than in layers I–V (recorded by rows 5 and 6). The rest of the electrodes did not record any observable events, because they were either not in the slice or were outside the neocortex. Some of these electrodes simultaneously recorded neural events of the same current source. This is because of the existence of a direct electrical connection between the exposed metalized parts of the electrodes on top of the brain slice through the thin layer of ACSF at the tissue–air interface.

The light-evoked seizure waves have very robust spatiotemporal propagation patterns. Figure 9 shows data averaged from eight separate waves. Two different optical powers of 5 mW and 15 mW were used, where 5 mW was near/at the threshold power to evoke epileptic waves. The overall delays in the case of the 5 mW stimulation are much longer than those from the 15 mW case, with larger standard deviations. This is consistent with previous observations in our laboratories. It can also be shown that the arrival time sequences at different electrodes are similar for the two different stimulation power levels, except for electrode 6.

6. Discussion and conclusion

We have designed, fabricated and demonstrated a novel hybrid device, integrating a tapered optical fiber (optrode) with a multi-electrode array, to demonstrate controlled optical stimulation and spatiotemporal recordings of optogenetically transfected cortical tissue *in vitro*. The single optrode construct has dual localized optical stimulation and electrical recording capability, which was demonstrated in mice retina. Although various optical fiber-

based light delivery methods have been previously reported [2,4,29], the present device offers further design possibilities and flexibility for controlling optical activation volume by changing the size of the optical aperture [37]. The optrode–MEA device has been able to map the 2D spatiotemporal propagation of light-induced epileptiform activity in mice slices. It has been demonstrated very recently that MEA itself can be used to record the microphysiology of epileptiform activity in human neocortex [44], showing its potential in clinical applications. Moreover, the optogenetic technology enables specific optical stimulation with respect to both cell type and cortical laminae [39]. Modulation of the initiation and propagation of epileptiform activities may thus be achieved by combining the optrode–MEA device with optogenetic methods, especially with the inhibitory light activated ion channel protein halorhodopsin (NpHR) [22].

Since the standard ‘non-optical’ MEAs used as the basis for our devices are extensively employed in *in vivo* extracellular recording, especially in primates [46], we suggest that our optrode–MEA constructs may also be applicable to *in vivo* brain structures such as the motor-cortex [1,27], where selective activation or suppression of neural activity could interfere with the dynamics of neural circuits. For *in vivo* work, we currently develop schemes where the optical fiber can be bundled together with the Au-electrical wiring from the array. Finally, multisite optical stimulation is also desirable for cortical layer or area specific modulation. The spatial resolution of multisite electrical stimulation is limited by the spread of the electric potential in the brain tissue [47]. We have shown elsewhere that matrix-addressable LED arrays with μm resolution can be coupled to multicore imaging fibers for spatiotemporally controlled optical excitations [53,54]. Such multicore fibers could perhaps be fabricated and integrated with multi-electrode arrays similar to optrode–MEA device for truly multisite spatiotemporal stimulation and recording of the neural activities.

Acknowledgments

Research supported by the National Institute of Health (NIBIB and NCMRR/NICHD) under Bioengineering Research Partnership Program (1R01EB007401-01), the Office of Naval Research under Neuroengineering Program (N0014-06-0185), the National Science Foundation under Biophotonics Program (0423566), and the Department of Energy. We thank Dr Olivia Dumitrescu for preparing the mouse retina tissue; Dr Kristen Richardson for useful discussion of picrotoxin experiments and Saundy Patrick for general technical support.

References

1. Achtman N, Afshar A, Santhanam G, Yu BM, Ryu SI, Shenoy KV. Free-paced high-performance brain–computer interfaces. J. Neural Eng 2007;4:336–347. [PubMed: 17873435]
2. Adamantidis AR, Zhang F, Aravanis AM, Deisseroth K, De Lecea L. Neural substrates of awakening probed with optogenetic control of hypocretin neurons. Nature 2007;450 420-U9.
3. Antosiewicz TJ, Szoplik T. Description of near- and far-field light emitted from a metal-coated tapered fiber tip. Opt. Exp 2007;15:7845–7852.
4. Aravanis AM, Wang LP, Zhang F, Meltzer LA, Mogri MZ, Schneider MB, Deisseroth K. An optical neural interface: *in vivo* control of rodent motor cortex with integrated fiberoptic and optogenetic technology. J. Neural Eng 2007;4:S143–S156. [PubMed: 17873414]
5. Badea T, Goldberg J, Mao BQ, Yuste R. Calcium imaging of epileptiform events with single-cell resolution. J. Neurobiol 2001;48:215–227. [PubMed: 11466708]
6. Beggs JM, Plenz D. Neuronal avalanches in neocortical circuits. J. Neurosci 2003;23:11167–11177. [PubMed: 14657176]
7. Bethe HA. Theory of diffraction by small holes. Phys. Rev 1944;66:163.
8. Betzig E, Trautman JK, Harris TD, Weiner JS, Kostelak RL. Breaking the diffraction barrier—optical microscopy on a nanometric scale. Science 1991;251:1468–1470. [PubMed: 17779440]

9. Bevilacqua F, Piguet D, Marquet P, Gross JD, Tromberg BJ, Depeursinge C. *In vivo* local determination of tissue optical properties: applications to human brain. Appl. Opt 1999;38:4939–4950. [PubMed: 18323984]
10. Blomstedt P, Hariz MI. Hardware-related complications of deep brain stimulation: a ten year experience. Acta Neurochir 2005;147:1061–1064.
11. Boyden ES, Zhang F, Bamberg E, Nagel G, Deisseroth K. Millisecond-timescale, genetically targeted optical control of neural activity. Nat. Neurosci 2005;8:1263–1268. [PubMed: 16116447]
12. Campagnola L, Wang H, Zyka MJ. Fiber-coupled light-emitting diode for localized photo stimulation of neurons expressing channelrhodopsin-2. J. Neurosci. Methods 2008;169:27–33. [PubMed: 18187202]
13. Campbell PK, Jones KE, Huber RJ, Horch KW, Normann RA. A silicon-based, 3-dimensional neural interface—manufacturing processes for an intracortical electrode array. IEEE Trans. Biomed. Eng 1991;38:758–768. [PubMed: 1937509]
14. Chagnacamitai Y, Connors BW. Horizontal spread of synchronized activity in neocortex and its control by gaba-mediated inhibition. J. Neurophysiol 1989;61:747–758. [PubMed: 2542471]
15. Chervin RD, Pierce PA, Connors BW. Periodicity and directionality in the propagation of epileptiform discharges across neocortex. J. Neurophysiol 1988;60:1695–1713. [PubMed: 3143812]
16. Connors BW. Initiation of synchronized neuronal bursting in neocortex. Nature 1984;310:685–687. [PubMed: 6147755]
17. Cruikshank SJ, Lewis TJ, Connors BW. Synaptic basis for intense thalamocortical activation of feedforward inhibitory cells in neocortex. Nat. Neurosci 2007;10:462–468. [PubMed: 17334362]
18. Drezet A, Woehl JC, Huant S. Far-field emission of a tapered optical fibre tip: a theoretical analysis. J. Microsc.-Oxf 2001;202:359–361.
19. Elstrott J, Anishchenko A, Greschner M, Sher A, Litke AM, Chichilnisky EJ, Feller MB. Direction selectivity in the retina is established independent of visual experience and cholinergic retinal waves. Neuron 2008;58:499–506. [PubMed: 18498732]
20. Flusberg BA, Cocker ED, Piyawattanametha W, Jung JC, Cheung ELM, Schnitzer MJ. Fiber-optic fluorescence imaging. Nat. Methods 2005;2:941–950. [PubMed: 16299479]
21. Flusberg BA, Nimmerjahn A, Cocker ED, Mukamel EA, Barretto RPJ, Ko TH, Burns LD, Jung JC, Schnitzer MJ. High-speed, miniaturized fluorescence microscopy in freely moving mice. Nat. Methods 2008;5:935–938. [PubMed: 18836457]
22. Gradinaru V, Thompson KR, Deisseroth K. eNpHR: a natronomonas halorhodopsin enhanced for optogenetic applications. Brain Cell Biol 2008;36:129–139. [PubMed: 18677566]
23. Gradinaru V, Thompson KR, Zhang F, Mogri M, Kay K, Schneider MB, Deisseroth K. Targeting and readout strategies for fast optical neural control *in vitro* and *in vivo*. J. Neurosci 2007;27:14231–14238. [PubMed: 18160630]
24. Grinvald A, Lieke E, Frostig RD, Gilbert CD, Wiesel TN. Functional architecture of cortex revealed by optical imaging of intrinsic signals. Nature 1986;324:361–364. [PubMed: 3785405]
25. Guillory KS, Normann RA. A 100-channel system for real time detection and storage of extracellular spike waveforms. J. Neurosci. Methods 1999;91:21–29. [PubMed: 10522821]
26. Hariz, MI. Complications of Deep Brain Stimulation Surgery. New York: Wiley-Liss; 2002. p. S162-S166.
27. Hochberg LR, Serruya MD, Friehs GM, Mukand JA, Saleh M, Caplan AH, Branner A, Chen D, Penn RD, Donoghue JP. Neuronal ensemble control of prosthetic devices by a human with tetraplegia. Nature 2006;442:164–171. [PubMed: 16838014]
28. Hoffmann, P.; Dutoit, B.; Salathe, RP. Comparison of Mechanically Drawn and Protection Layer Chemically Etched Optical Fiber Tips. Amsterdam: Elsevier Science; 1995. p. 165-170.
29. HuberDPetreanuLGhitaniNRanadeSHromadkaTMainenZSvobodaKSparse optical microstimulation in barrel cortex drives learned behaviour in freely moving mice. Nature 62008451
30. Jones KE, Campbell PK, Normann RA. A glass silicon composite intracortical electrode array. Ann. Biomed. Eng 1992;20:423–437. [PubMed: 1510294]

31. Lazebnik M, Marks DL, Potgieter K, Gillette R, Boppart SA. Functional optical coherence tomography for detecting neural activity through scattering changes. Opt. Lett 2003;28:1218–1220. [PubMed: 12885026]
32. Lewis A, Isaacson M, Harootunian A, Muray A. Development of a 500-a spatial-resolution light-microscope. 1. Light is efficiently transmitted through gamma-16 diameter apertures. Ultramicroscopy 1984;13:227–231.
33. Mayberg HS, Lozano AM, Voon V, McNeely HE, Seminowicz D, Hamani C, Schwalb JM, Kennedy SH. Deep brain stimulation for treatment-resistant depression. Neuron 2005;45:651–660. [PubMed: 15748841]
34. Miles R, Wong RKS. Single neurons can initiate synchronized population discharge in the hippocampus. Nature 1983;306:371–373. [PubMed: 6316152]
35. Nagel G, Szellas T, Huhn W, Kateriya S, Adeishvili N, Berthold P, Ollig D, Hegemann P, Bamberg E. Channelrhodopsin-2, a directly light-gated cation-selective membrane channel. Proc. Natl Acad. Sci. USA 2003;100:13940–13945. [PubMed: 14615590]
36. Nordhausen CT, Maynard EM, Normann RA. Single unit recording capabilities of a 100 microelectrode array. Brain Res 1996;726:129–140. [PubMed: 8836553]
37. Obermuller C, Karrai K. Far-field characterization of diffracting circular apertures. Appl. Phys. Lett 1995;67:3408–3410.
38. Perlmutter JS, Mink JW. Deep brain stimulation. Ann. Rev. Neurosci 2006;29:229–257. [PubMed: 16776585]
39. Petreanu L, Huber D, Sobczyk A, Svoboda K. Channelrhodopsin-2-assisted circuit mapping of long-range callosal projections. Nat. Neurosci 2007;10:663–668. [PubMed: 17435752]
40. Pinto DJ, Patrick SL, Huang WC, Connors BW. Initiation, propagation, and termination of epileptiform activity in rodent neocortex *in vitro* involve distinct mechanisms. J. Neurosci 2005;25:8131–8140. [PubMed: 16148221]
41. Piyawattanametha W, Barretto RPJ, Ko TH, Flusberg BA, Cocker ED, Ra HJ, Lee DS, Solgaard O, Schnitzer MJ. Fast-scanning two-photon fluorescence imaging based on a microelectromechanical systems two-dimensional scanning mirror. Opt. Lett 2006;31:2018–2020. [PubMed: 16770418]
42. Pohl DW, Denk W, Lanz M. Optical stethoscopy—image RECORDING with resolution lambda/20. Appl. Phys. Lett 1984;44:651–653.
43. Robinson DA. The electrical properties of metal microelectrodes. Proc. IEEE 1968;56:1065–1071.
44. Schevon CA, Ng SK, Cappell J, Goodman RR, McKhann G, Waziri A, Branner A, Sosunov A, Schroeder CE, Emerson RG. Microphysiology of epileptiform activity in human neocortex. J. Clin. Neurophysiol 2008;25:321–330. [PubMed: 18997628]
45. Schwartzkroin PA, Prince DA. Cellular and field potential properties of epileptogenic hippocampal slices. Brain Res 1978;147:117–130. [PubMed: 656907]
46. Serruya MD, Hatsopoulos NG, Paninski L, Fellows MR, Donoghue JP. Instant neural control of a movement signal. Nature 2002;416:141–142. [PubMed: 11894084]
47. Shimada A, Kasai N, Wada M, Nakano N, Torimitsu K. Multisite stimulation pattern for a higher density microelectrode array. Neurosci. Res 2008;61 S252-S.
48. Tian N, Copenhagen DR. Visual stimulation is required for refinement of ON and OFF pathways in postnatal retina. Neuron 2003;39:85–96. [PubMed: 12848934]
49. Traub, RD.; Miles, R. Neuronal Networks of the Hippocampus. Cambridge, NY: Cambridge University Press; 1991.
50. Traub RD, Wong RKS. Cellular mechanism of neuronal synchronization in epilepsy. Science 1982;216:745–747. [PubMed: 7079735]
51. Williams JC, Rennaker RL, Kipke DR. Long-term neural recording characteristics of wire microelectrode arrays implanted in cerebral cortex. Brain Res. Protoc 1999;4:303–313.
52. Wong RKS, Traub RD. Synchronized burst discharge in disinhibited hippocampal slice. 1. Initiation in CA2–CA3 region. J. Neurophysiol 1983;49:442–458. [PubMed: 6300343]

53. Xu H, Davitt KM, Dong W, Song YK, Patterson WR, Aizenman CD, Nurmikko AV. Combining multicore imaging fiber with matrix addressable blue/green LED arrays for spatiotemporal photonic excitation at cellular level. IEEE J. Sel. Top. Quantum Electron 2008;14:167–170.

54. Xu H, Zhang J, Davitt KM, Song YK, Nurmikko AV. Application of blue-green and ultraviolet micro-LEDs to biological imaging and detection. J. Phys. D: Appl. Phys 2008;41:13.

55. Yaroslavsky AN, Schulze PC, Yaroslavsky IV, Schober R, Ulrich F, Schwarzmaier HJ. Optical properties of selected native and coagulated human brain tissues *in vitro* in the visible and near infrared spectral range. Phys. Med. Biol 2002;47:2059–2073. [PubMed: 12118601]

56. Zhang F, Wang LP, Brauner M, Liewald JF, Kay K, Watzke N, Wood PG, Bamberg E, Nagel G, Gottschalk A, Deisseroth K. Multimodal fast optical interrogation of neural circuitry. Nature 2007;446 633-U4.

57. Zhang YP, Oertner TG. Optical induction of synaptic plasticity using a light-sensitive channel. Nat. Methods 2007;4:139–141. [PubMed: 17195846]

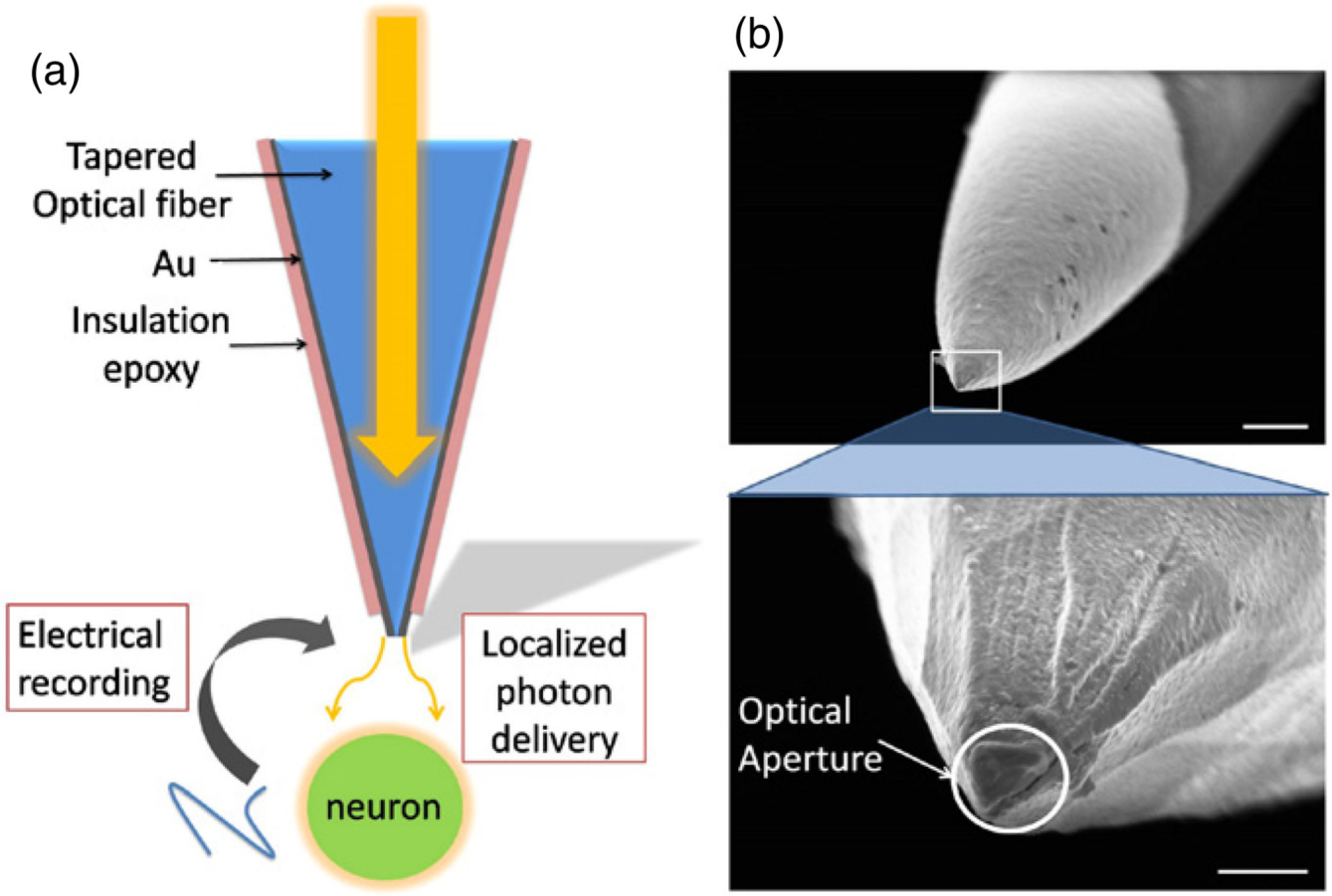

Figure 1.
Single optrode with dual stimulation and recording functions. (a) Concept schematic. Light is locally delivered through the aperture at the tip of the tapered optical fiber to nearby neurons; the neuronal activities are recorded through the thermally metalized gold tip of the optrode. (b) SEM images of the optrode tip. The exposed metallic part of the tip is approximately 50 μm, appearing brighter in the upper image. The diameter of the optical aperture (outlined in white circle) is about 1 μm in the lower image. Scale bars are 10 μm and 1 μm for the upper and lower images.

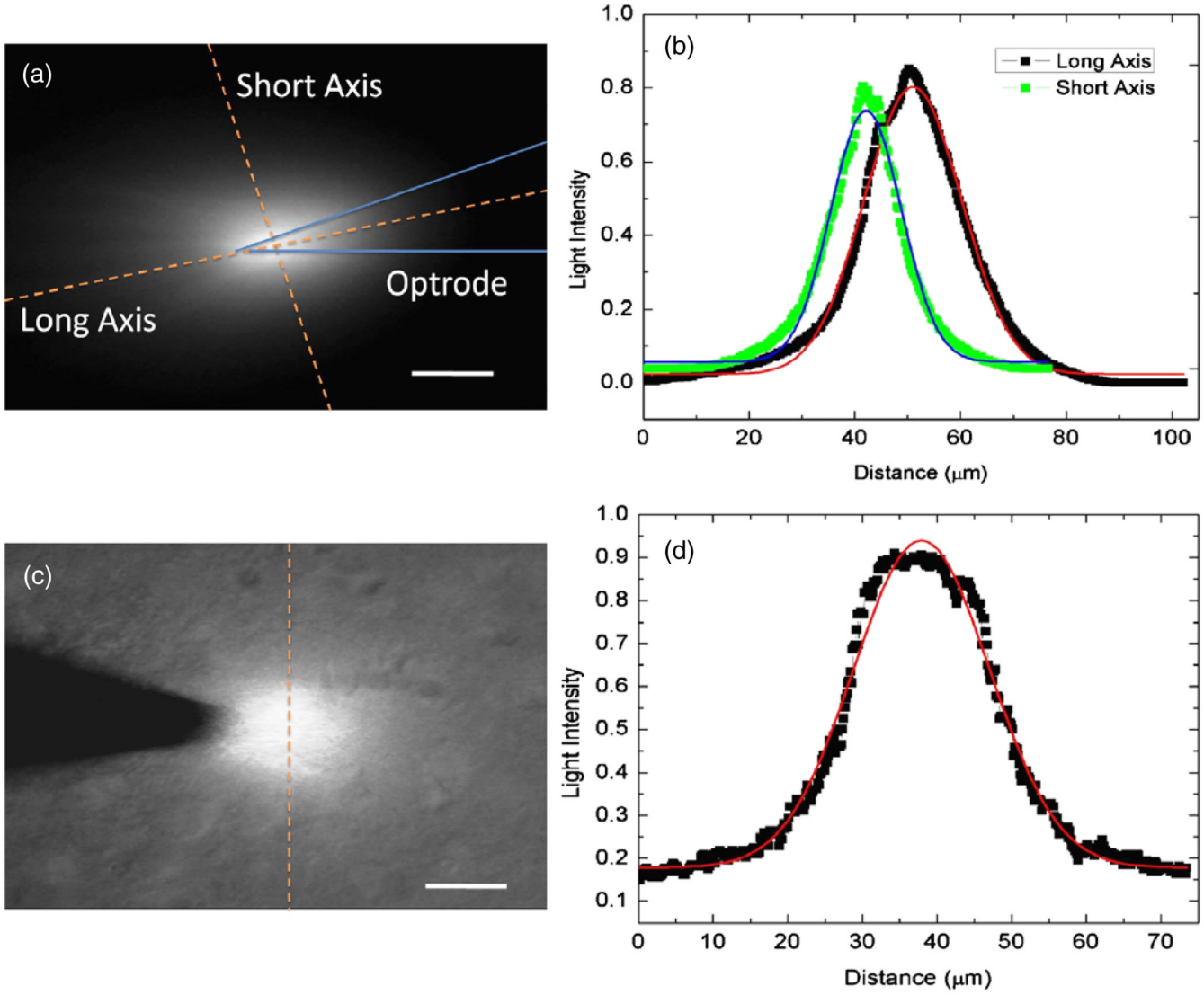

Figure 2.

Optical characteristics of the optrode. (a) The solution-based Rhodamine-6G fluorescence image of the optrode output excited by a 532 nm laser. Blue lines guide the eye for outlining the optrode, and the orange dotted lines define the ‘short’ and ‘long’ axes along which the intensity distributions are analyzed. (b) The relative fluorescence intensity distribution along the short and long axes. The solid red and blue lines are the Gaussian fits, with variances of 18 μm for the long axis and 13 μm for the short axis. (c) A DIC image of the scattered 440 nm light from the optrode in a mouse brain slice. The orange dotted line shows the axis along which the intensity distribution is analyzed. (d) The relative scattered intensity distribution and the corresponding Gaussian fit, with a variance of 18 μm. The scale bars in both (a) and (c) are 20 μm.

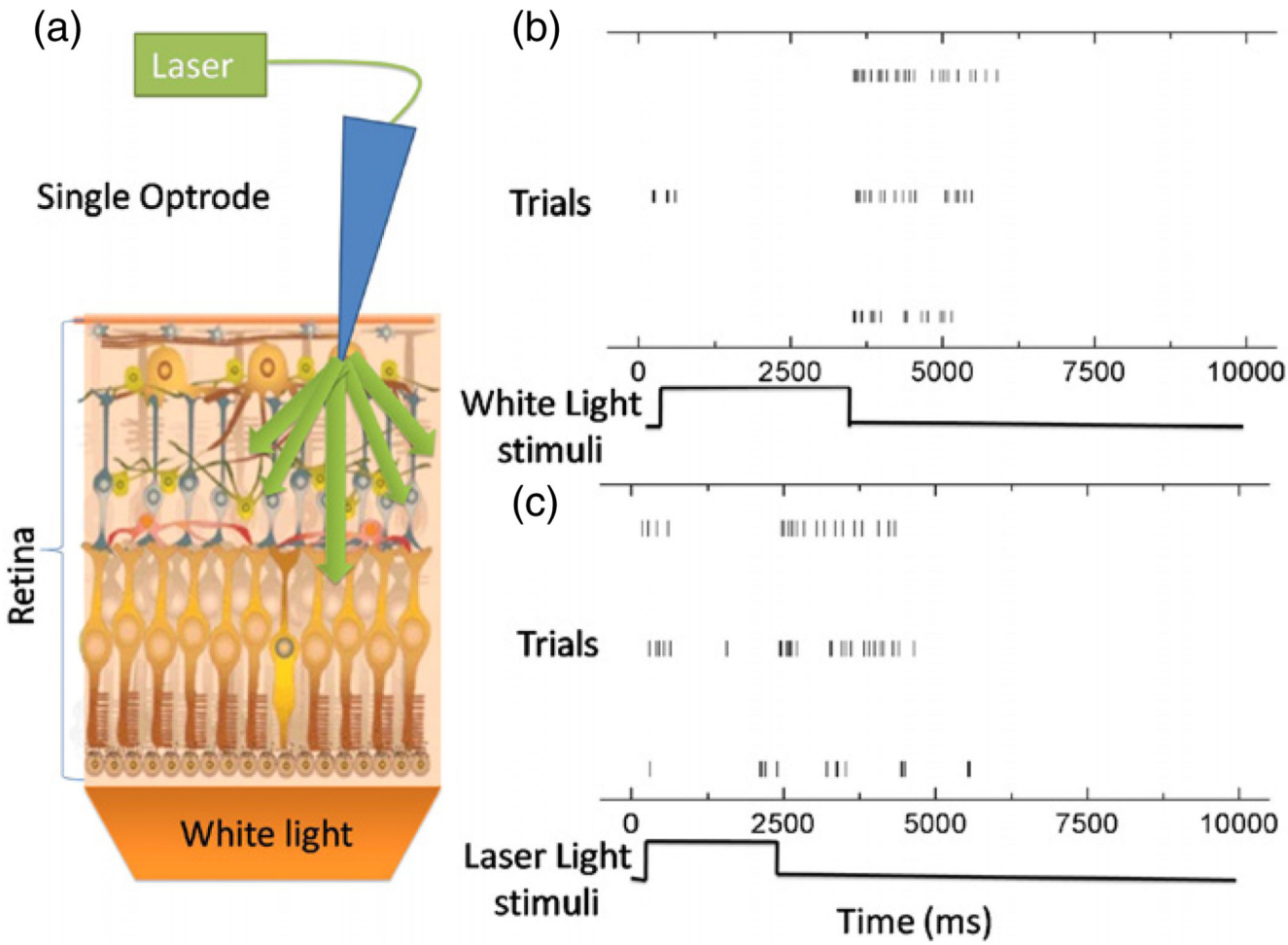

Figure 3.

Optical stimulation and electrical recording using a stand-alone optrode in a *mouse retina*. (a) Schematic of the experiment. The single optrode records spiking activity from ganglion cells, which are optically stimulated by unguided uniform white light and optical fiber guided 532 nm laser light through the optrode, respectively. The schematic image for mouse retina was obtained from http://gsbs.uth.tmc.edu/images/klein_diagram.jpg (b) Raster plots of one ganglion cell response to white light stimuli of approximately 2.5 s duration. The results from three trials for the same neuron have been shown. (c) Raster plots of another ganglion cell response to an optrode-guided 532 nm green laser light stimulus (~2 s pulses). The results from three trials for the same neuron are shown. Spike sorting was done on all the recorded waveforms in (b) and (c), which were taken from the same specimen.

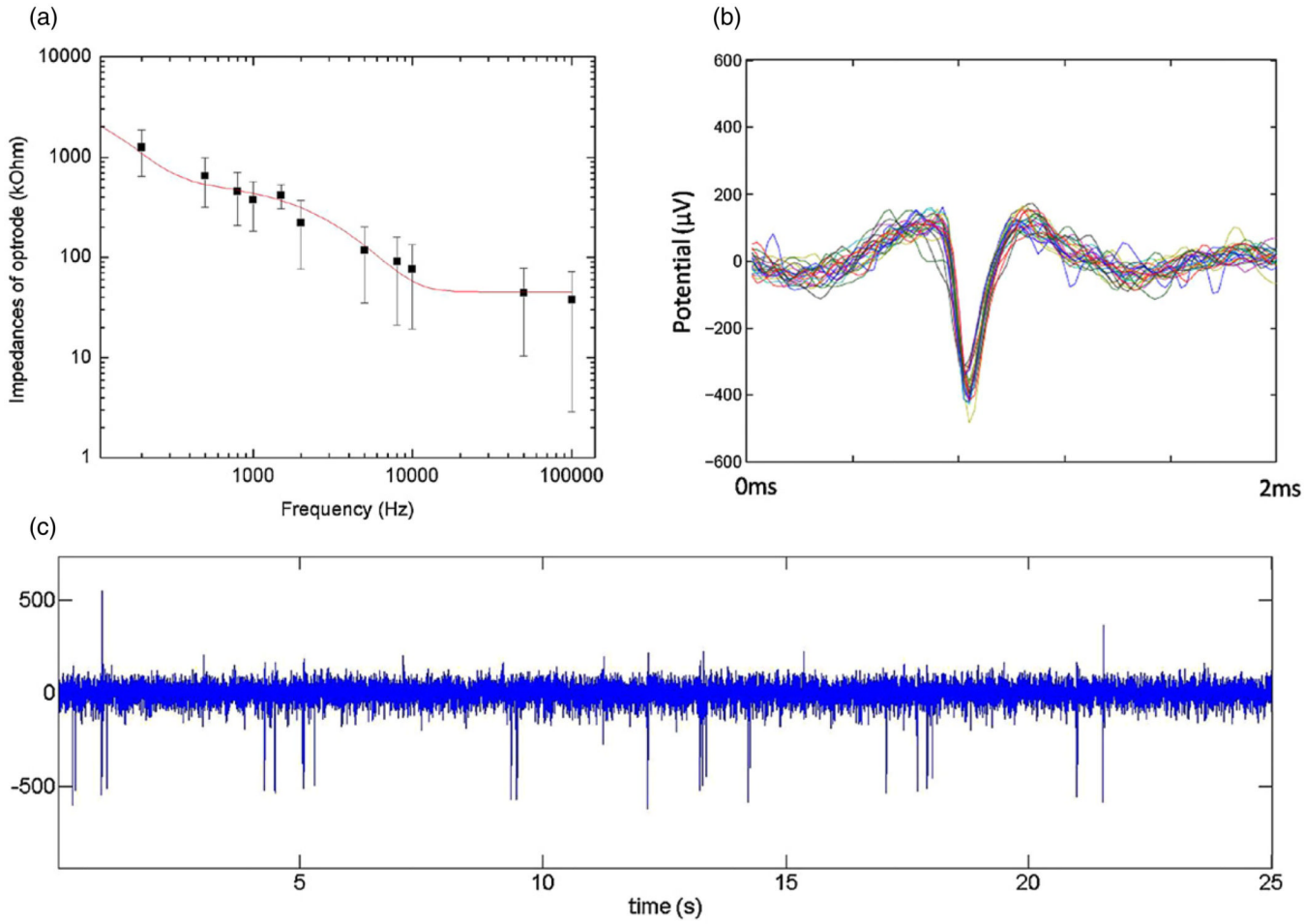

Figure 4.

Electrical recording characteristics of optrode from retinal ganglion neurons in figure 3. (a) The average impedance spectrum of eight separately fabricated optrodes measured in PBS. The impedances at $f = 1$ kHz lie between 112 kΩ and 671 kΩ. The solid line is the double exponential fit of the average impedance. (b) 24 spike waveforms from mouse retinal ganglion cells overlaid in a 2 ms window. All signals are bandpass-filtered at 250 Hz–4.8 kHz and thresholded at −300 μV. (c) The full bandwidth (10 kHz) data for (b). The V_{pp} for recorded spikes are in the range of 100–500 μV. The unit for the vertical axis is expressed in μV.

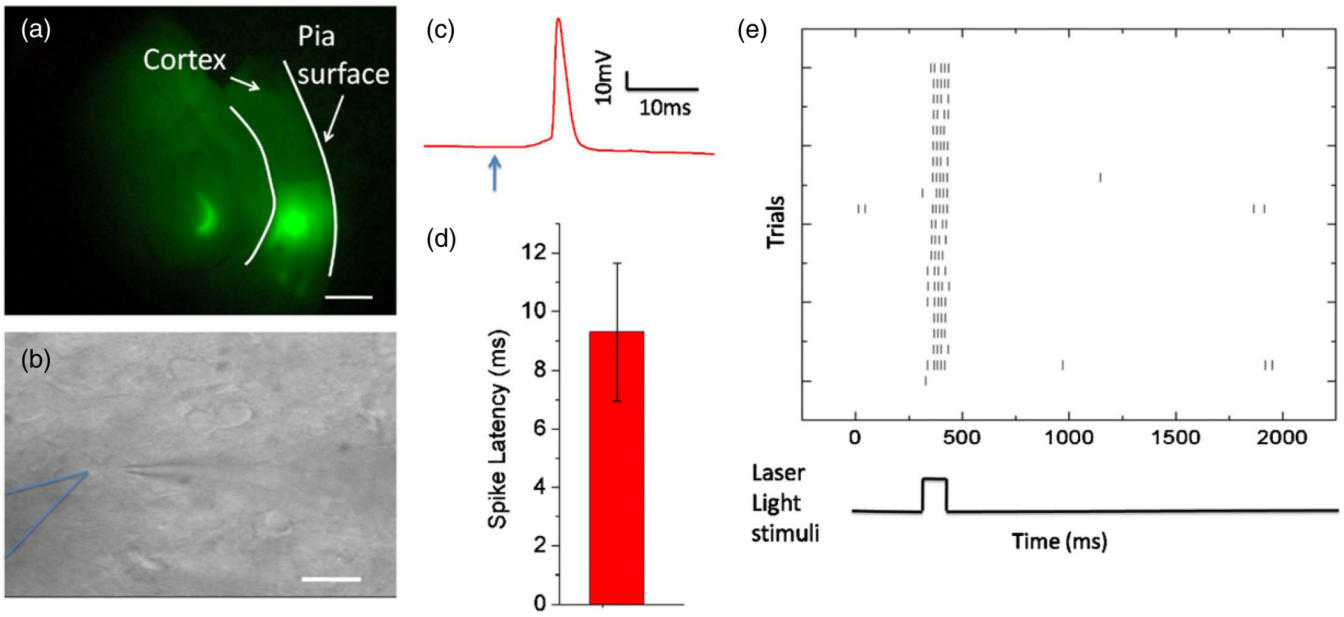

Figure 5.

Photostimulation of ChR2-positive neocortical pyramidal neuron by single optrode. (a) EYFP fluorescence in a coronal slice from a transfected mouse. Scale bar is 1 mm. (b) DIC image showing the tip of the optrode and the patch pipette on a given fluorescent neuron—the single optrode is located 50 μm above the patched neuron (outlined in blue). Scale bar is 20 μm. (c) Onset action potential triggered by the optrode. Blue arrow indicates the switching of the laser light of 3.3 mW power and 10 ms duration. (d) The spike latencies (*n* = 22) of action potentials triggered by 3.3 mW, 10 ms laser pulses. (e) Sample raster plot of spikes triggered by 100 ms, 6.6 mW laser pulses. The interval between each trial is 60 s.

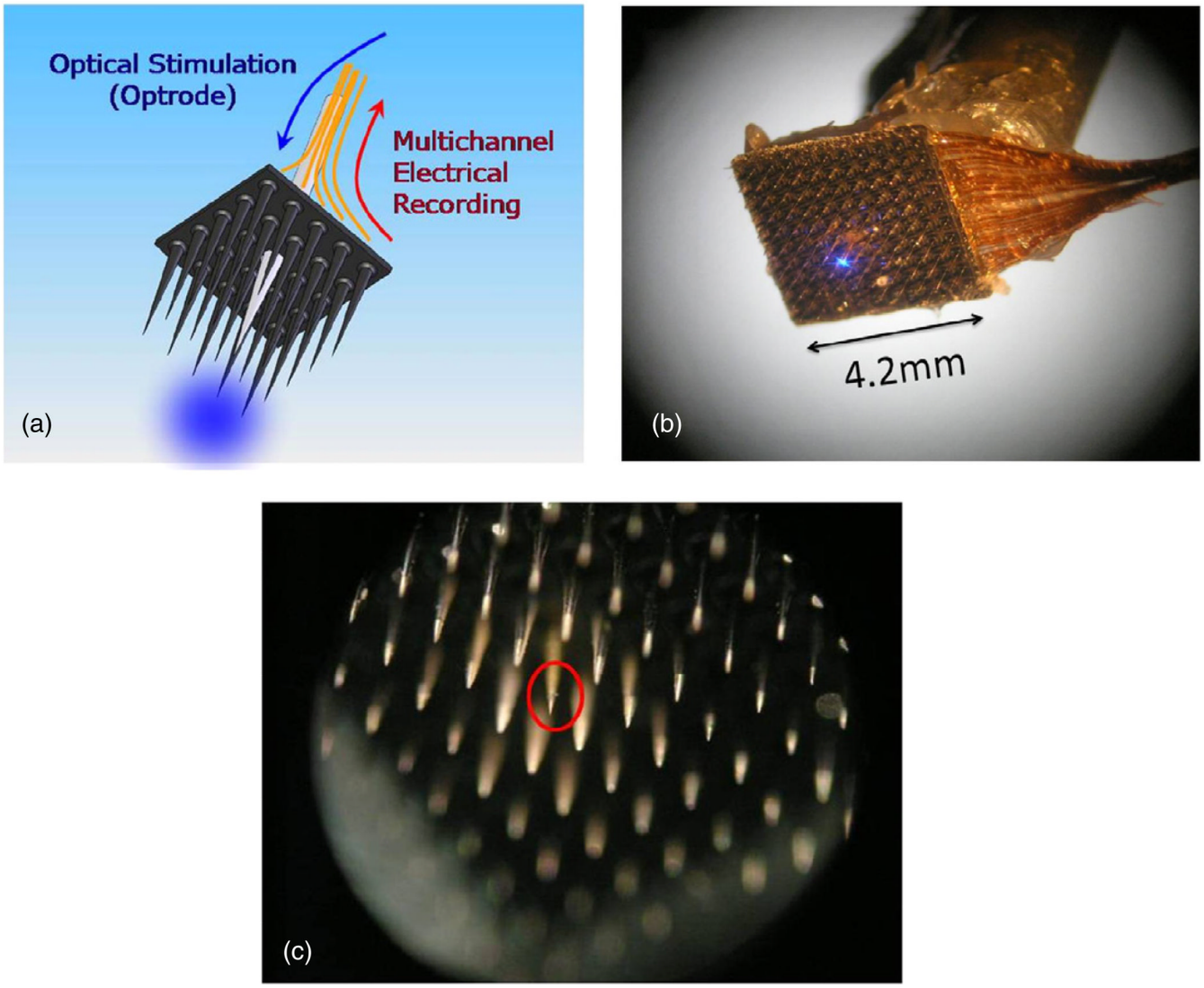

Figure 6.
Assembled optrode–MEA device. (a) Schematic of the device. The optrode is coupled to the MEA through a laser drilled hole, replacing one of the silicon microelectrodes. (b) An optical microscope image of the device, showing blue laser light emanating from the tip of the optrode. (c) A close-up view of the tips of the electrodes, where the red circle identifies the optrode. The spacing between each two neighboring electrodes is 400 μm.

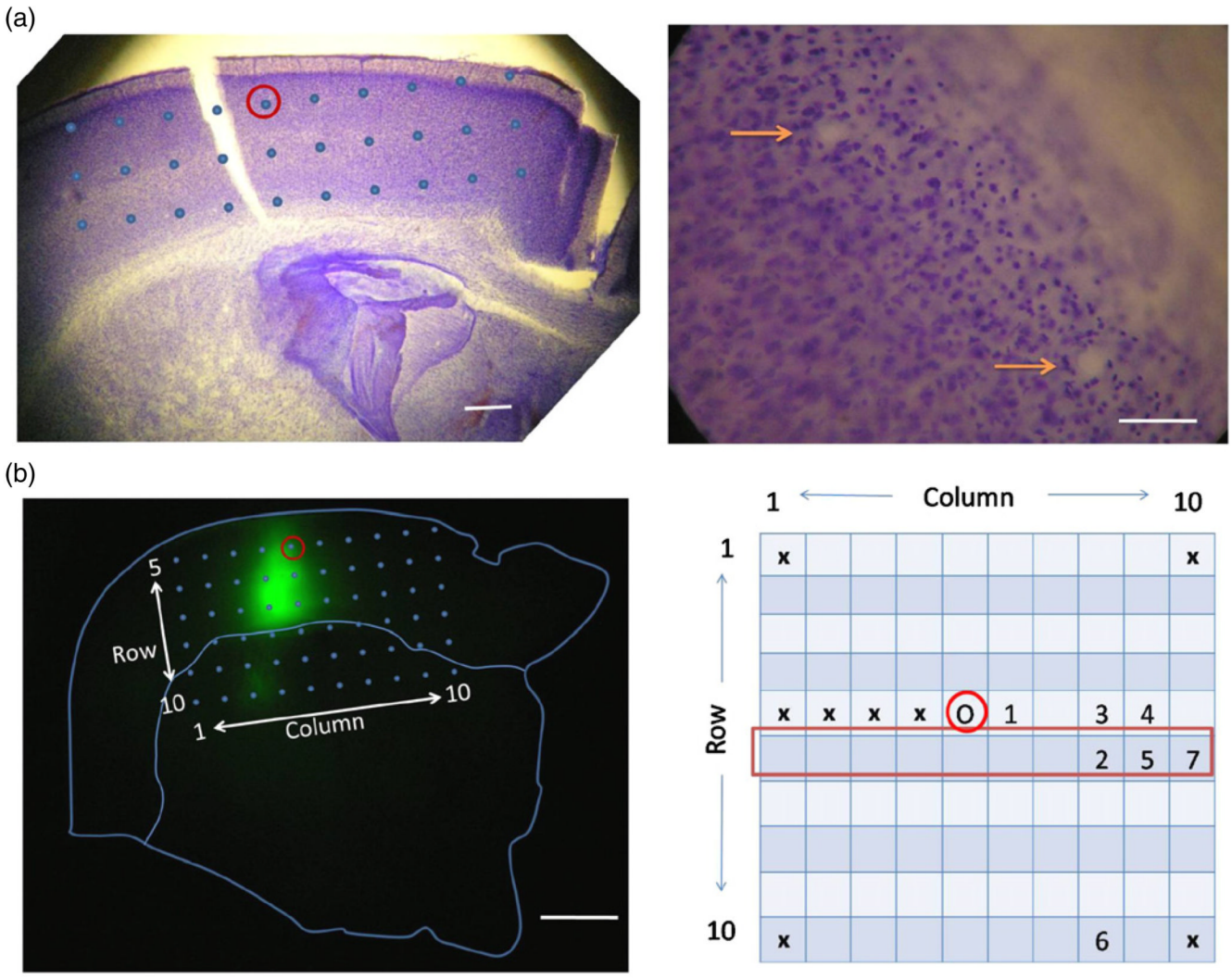

Figure 7.

Layout of multielectrode array in a ChR2 transfected slice. (a) Histology of the ChR2 transfected slice with Nissl staining shows the locations of the electrodes in the neocortex. The red circle represents the position of the optrode. The orange arrows indicate the 'markers' which are created upon insertion of the electrodes into the tissue. The scale bars are 400 μm for the left panel and 100 μm for the right panel. (b) EYFP fluorescence and the positions of the electrodes in the coronal slice. The outlines of the entire slice and the neocortex are sketched in blue. The 100 elements of the multi-electrode array are numbered from columns 1–10 and rows 1–10. The red circle in the left panel and the letter 'O' in the right panel represent the position of the optrode. The 'x' electrodes are left unwired. Scale bar is 1 mm.

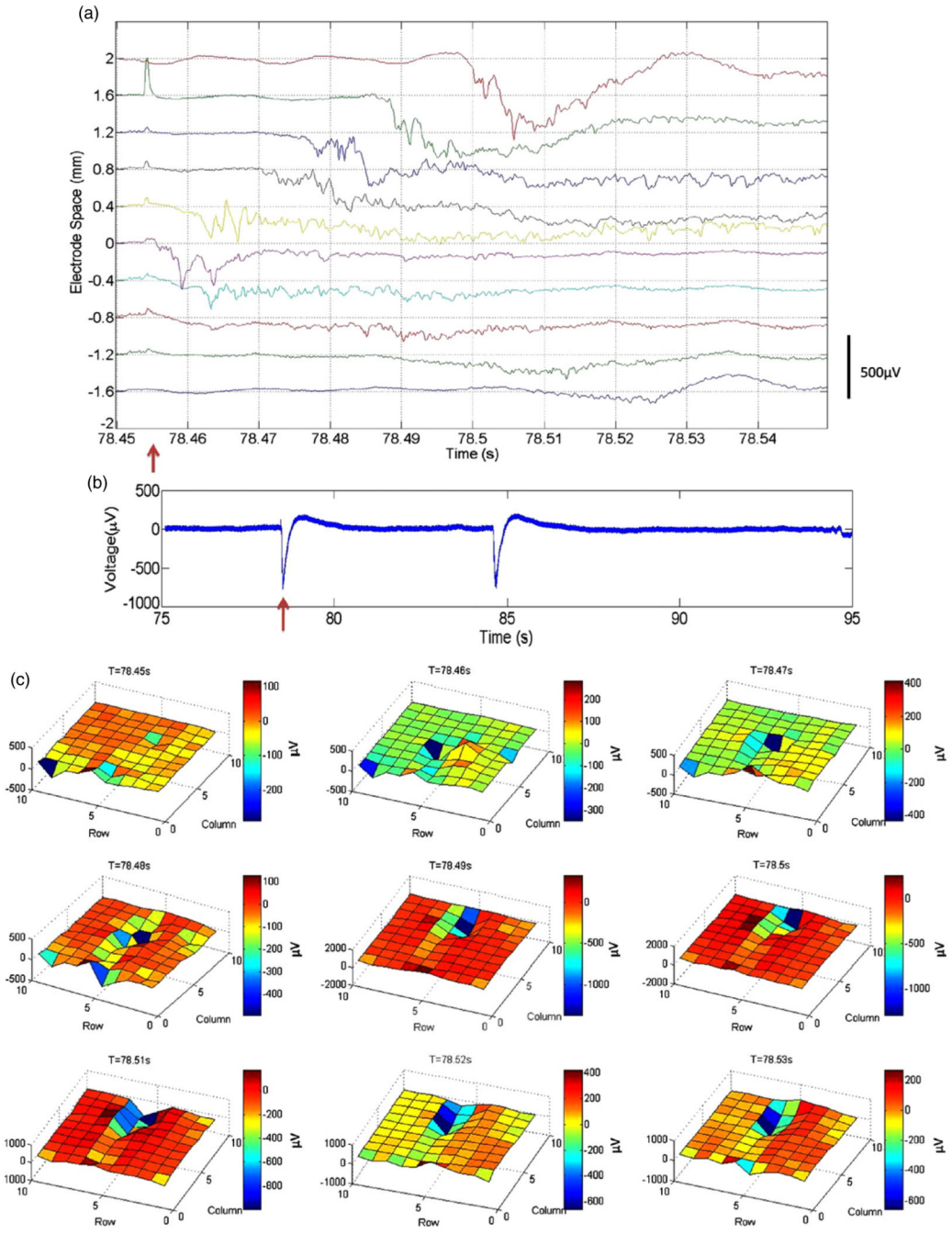

Figure 8.

Photostimulation of epileptic events and their spatiotemporal propagation demonstrating the utility of the optrode–MEA device concept. (a) Propagation of the epileptic wave in row 6. The light stimulus was on at 78.454 s with a duration of 500 μs and a power of 15 mW, indicated by the red arrow. The electrode at location '0' in the figure is in column 5. (b) The complete waveform of the electrode at '0.8' mm offset from the optrode in (a). The red arrow indicates the onset of the light stimulus. The second wave in the plot is a spontaneously occurring one. (c) The spatiotemporal propagation of an epileptic wave. The row and column numbers refer to the position of the electrodes in figure 7(b), right panel. The light triggered epileptic wave first appears in the frame at T = 78.46 s at row 6 column

5. It propagates in both the columns and the rows. Large field potential events can be seen along rows 5 and 6.

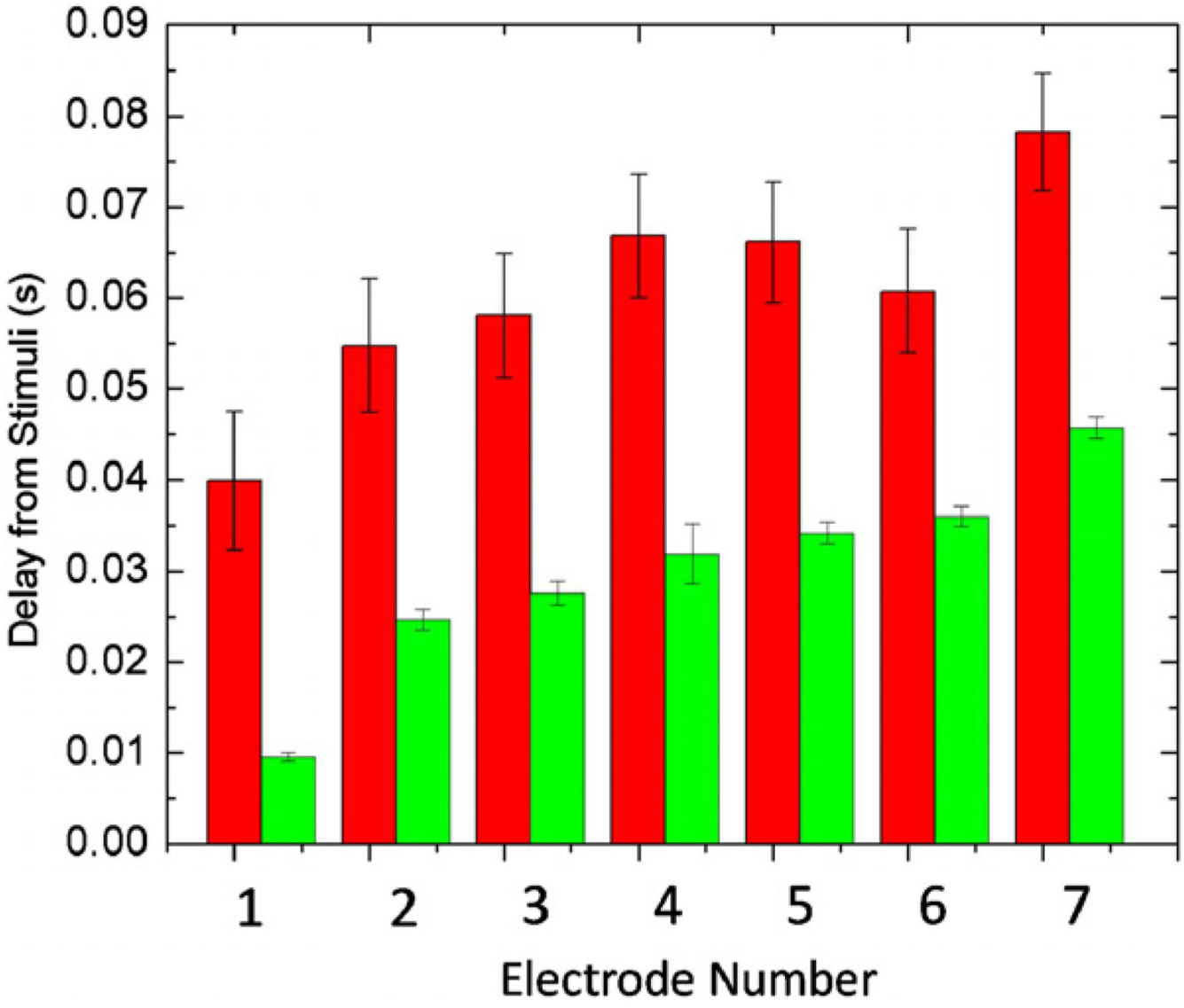

Figure 9.
The repetitiveness of the spatiotemporal patterns of light-stimulated epileptic events. The electrode numbers in the *x* axis refer to the positions of the electrodes in figure 7(b), right panel. Red columns of each channel are the delays from 5 mW light stimuli, while green columns are those from 15 mW light stimuli.